American Mineralogist
Vol. 57, pp. 1210–1231 (1972)

STABILITY OF ACMITE–JADEITE PYROXENES AT LOW PRESSURE

R. K. Popp and M. C. Gilbert, *Department of Geological Sciences, Virginia Polytechnic Institute and State University, Blacksburg, Virginia 24061*

Abstract

Hydrothermal experiments in the system $NaFeSi_2O_6$ (acmite + quartz)–$NaAlSi_2O_6$ (albite, or jadeite + quartz) have defined the curve separating the stability fields of clinopyroxene + quartz from clinopyroxene + albite + quartz. At 600°C and 4 kbar in the silica-saturated system, the maximum extent of jadeite solubility in sodic, Fe–Al, clinopyroxenes is between 4 and 5 mol percent jadeite. At 500°C and 4 kbar, the maximum solubility occurs between 5 and 6 mol percent jadeite. These results are consistent with an ideal solution model for the sodic pyroxenes based on a pressure of breakdown of pure albite to jadeite + quartz of 16.7 kb at 600°C and of 14.5 kbar at 500°C. If there is solubility of iron–albite in albite at 600°C, it is probably less than 4 to 5 mol percent.

Acmitic pyroxenes occurring in low-pressure, high-temperature, silica-saturated environments such as alkali granites and related pegmatites will be lowest in jadeite component. Acmitic pyroxenes in silica-undersaturated igneous rocks should show appreciably more jadeite component if they equilibrated with albite and nepheline. For the silica-saturated case, acmitic pyroxene can show high jadeite component only in high-pressure, low-temperature environments. Acmitic pyroxenes co-existing with albite and quartz might be used as a pressure indicator if an independent estimate of temperature can be made.

Introduction

In recent years, considerable attention has been focused on the genesis of pyroxenes occurring along the join $NaAlSi_2O_6$ (jadeite)–$NaFe^{3+}Si_2O_6$ (acmite). These pyroxenes (1) are important minerals in blueschist metamorphic terranes (Ernst and others, 1970); (2) represent important end member constituents of omphacites—a major phase in eclogites (Clark and Papike, 1968); and (3) are characteristic of some alkali-rich igneous rocks (Bailey, 1969).

Previous experimental and theoretical studies have been concerned largely with the Al-rich portion of the join. The three reactions of petrological significance used to explain the genesis of jadeite are:

$$\underset{\text{albite}}{NaAlSi_3O_8} \rightarrow \underset{\text{jadeite}}{NaAlSi_2O_6} + \underset{\text{quartz}}{SiO_2} \qquad (1)$$

$$\underset{\text{nepheline}}{NaAlSiO_4} + \underset{\text{albite}}{NaAlSi_3O_8} \rightarrow \underset{\text{jadeite}}{2NaAlSi_2O_6} \qquad (2)$$

$$\underset{\text{analcite}}{NaAlSi_2O_6 \cdot H_2O} \rightarrow \underset{\text{jadeite}}{NaAlSi_2O_6} + H_2O \qquad (3)$$

Studies on the Fe–rich end of the join have been limited to pure acmite compositions (Gilbert, 1969; Bailey, 1969). Gilbert (1967) determined cell parameters for pyroxenes synthesized part way across the jadeite–acmite join. The effect of substitution of Fe^{3+} for Al^{3+} on the phase relations of sodic pyroxenes along the join $NaAlSi_3O_8$–$NaFeSi_3O_8$ (Fig. 1) on reaction (1) has been investigated experimentally up to 40 mole percent Fe^{3+} by Newton and Smith (1967), and theoretically by Essene and Fyfe (1967). From these studies the general form of the system at constant temperature is as shown in Figure 2.

The purpose of the present study was to determine the location of the phase boundary in Figure 2 at the iron–rich side of the join at pressures in the range attainable in cold–seal hydrothermal apparatus. Location of the field boundary in this range may serve as a test for the ideality of the jadeite–acmite solid solution series providing the *P–T* breakdown of pure albite is assumed to be accurately known.

Crystal Chemistry

Cell parameters for the end member compositions have been reported previously as:

	Jadeite (Prewitt & Burnham, 1966)	Acmite (Nolan & Edgar, 1963)
a (Å)	9.418 (1)	9.658 (2)
b (Å)	8.562 (2)	8.795 (2)
c (Å)	5.219 (1)	5.294 (1)
β (°)	107.58 (1)	107.42 (2)
V (Å^3)	401.20 (15)	429.1 (1)

These values agree with those of Gilbert (1967), who found essentially a straight line relationship between composition and cell parameters of pyroxenes synthesized at high pressure on the jadeite–acmite join, and with those of pure acmite synthesized in this study (see table 2).

The pyroxenes jadeite and acmite exhibit $C2/c$ space group symmetry and are isostructural with diopside as determined by Warren and Bragg (1928). The structure of jadeite has since been refined by Prewitt and Burnham (1966) and that of acmite by Clark and others (1969). Because the pyroxenes on the jadeite–acmite join differ only by substitution of Fe^{3+} for Al^{3+} in the $M(1)$ sites, any differences in cell parameters should be due to differences in the sizes of these two cations. The a and b cell edges of acmite are greater than those of jadeite by 0.240 and 0.233 Å, respectively. Shannon and Prewitt (1969) give ionic radii for sixfold coordination as: Al^{3+} = 0.530 Å, Fe^{3+}

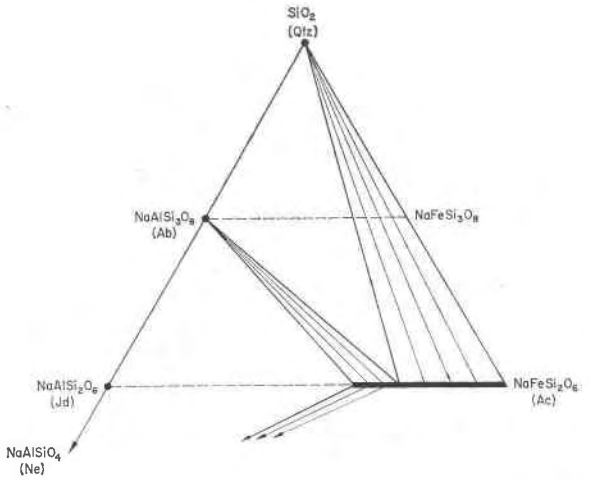

FIG. 1. Schematic isothermal, isobaric diagram for a portion of the system SiO_2–$NaAlSiO_4$–$NaFeSiO_4$. The join $NaAlSi_3O_8$–$NaFeSi_3O_8$ was investigated in this study.

(high spin) = 0.645 Å. As a line passing through the unit cell parallel to a or parallel to b intersects only one $M(1)$ atom, the difference in diameter between these two ions, 0.230 Å, is approximately the same size as the difference in the a and b cell edges. Based on the success of these simple geometrical considerations in explaining cell geometry, it is not surprising that ideal–solution models have been found workable when applied to acmite–jadeite pyroxenes.

In contrast to the idea solution model, Dobretsov (1962) suggested the existence of a solvus located between Ac_{40} and Ac_{80} based on the compositions of naturally occurring pyroxenes. Since his solvus on the Jd–Ac join is based upon compositional gaps rather than coexisting pyroxenes, it may be a reflection of P–T requirements indicated in Figure 2 along with natural chemical control. No such solvus has been reported from experimental studies. In addition, Essene and Fyfe (1967) have reported pyroxene compositions falling in the center of Dobretsov's solubility gap.

CALCULATED PHASE DIAGRAM

The phase diagram at constant temperatures for the system $NaFeSi_3O_8$–$NaAlSi_3O_8$, treated ideally, may be calculated using the equation

$$RT \ln \frac{X_{Jd}^{Px}}{X_{Ab}^{Pc}} = \Delta\overline{V}\,\Delta P, \qquad (4)$$

where X_{Jd}^{Px} is the mole fraction of $NaAlSi_2O_6$ component in the pyroxene, X_{Ab}^{Pc} is the mole fraction of $NaAlSi_3O_8$ in the plagioclase, $\Delta\overline{V}$ is the molar volume of the pure jadeite–pure albite reaction and is assumed to be pressure independent, and ΔP is the pressure difference between the pure jadeite–pure albite equilibrium and the given solid solution reaction. Similar approaches were used by Newton and Smith (1967) and Essene and Fyfe (1967).

A number of values for $\Delta\overline{V}$ for the reaction Ab $\rightleftarrows$ Jd + Qtz have been cited in the literature. The $\Delta\overline{V}$ used here (16.98 $\pm$ .19 cm^3) was calculated using the molar volumes of low albite, low quartz, and

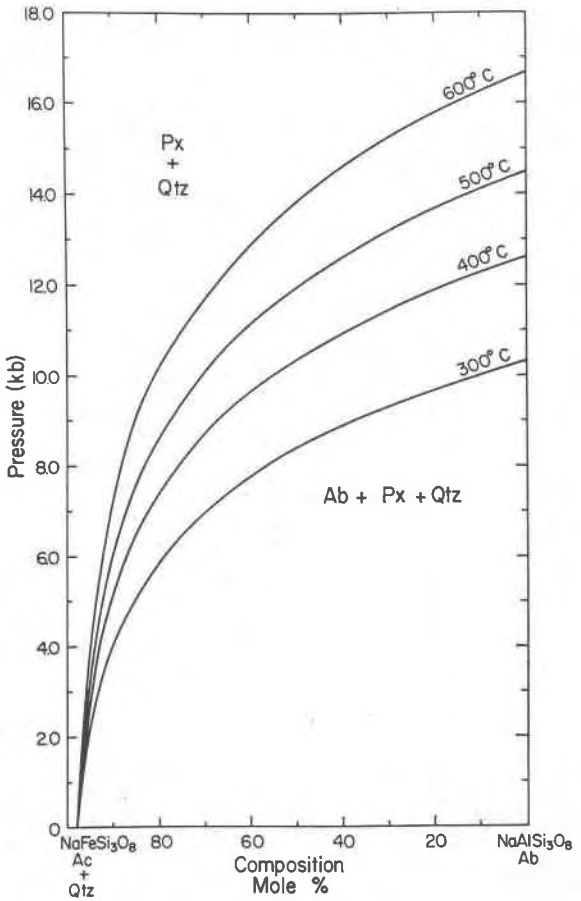

FIG. 2. *P–X* plot of phase relations in the system $NaAlSi_3O_8$–$NaFeSi_3O_8$, assuming ideality. Pressures of pure albite breakdown were taken from Figure 3.

jadeite tabulated by Robie and others (1967). If compressibility and thermal expansion of the phases were considered, the $\Delta\overline{V}$ at 12 kbar and 400°C would be about 1 cm^3 smaller than the $\Delta\overline{V}$ used. Substitution of the appropriate values in equation (4) gives:

$$\ln \frac{X_{Jd}^{Px}}{X_{Ab}^{Pc}} = \frac{\Delta P}{T} \frac{16.98}{.083147} \frac{cm^3\ mole^{-1}}{cm^3\ kb\ deg^{-1}\ mole^{-1}}$$

$$\ln \frac{X_{Jd}^{Px}}{X_{Ab}^{Pc}} = \left(204.216 \frac{deg}{kb}\right)\left(\frac{\Delta P}{T}\right) \tag{5}$$

The problem of calculation is thus reduced to determination of the equilibrium pressure of the reaction Ab $\rightleftarrows$ Jd + Qtz at the desired temperatures. M. S. Newton and Kennedy (1968), R. C. Newton and Smith (1967), Boettcher and Wyllie (1968), and Birch and Lecomte (1960) have studied this reaction in the 400–1000°C range. A plot of the pertinent data along with the pressure and temperatures uncertainties for the 400–650°C range is given in Figure 3.[1] Higher temperature data were omitted because of the steepening effect the high–low albite transition will have on the *P–T* slope of the curve. The high–low albite transition is believed to take place over the range 500–700°C (Hlabse and Kleppa, 1968; Boettcher and Wyllie, 1968).

All of the studies used in Figure 3 were carried out in piston–cylinder devices, and thus there may be pressure discrepancies incorporated due to the non–hydrostatic nature of the solid pressure medium (Richardson *et al.*, 1968). In addition, part of the pressure differences may be due to the differing frictional corrections applied. Given the data and estimated uncertainties in Figure 3, slopes of the reaction curve can vary considerably. The curve was drawn essentially to satisfy the brackets of Newton and Smith, and Boettcher and Wyllie. Attempting to locate the pressure of reaction by averaging the midpoints of the data in Figure 3 led to inconsistent results which suggest that Newton and Kennedy's brackets may be located at pressures slightly too high. Using the Clapeyron equation, thermal expansion and compressibility data from Clark (1966), and the relation $(\partial S/\partial P)_T = -(\partial V/\partial T)_P$, a slope of 20.2 bar/deg was calculated at 400°C and 12.3 kbar. The slope measured from Figure 3 is 21.8 bar/deg. The difference is within the un-

[1] After this study was completed, an inter-laboratory comparison of the determination of the pressure of albite breakdown to jadeite plus quartz in piston–cylinder apparatus was published (Johannes and others, 1971). On the basis of six determinations using Burma jade, natural quartz, and synthetic high albite, the average pressure of albite breakdown at 600°C was 16.25 ± .5 kb. The value used in this study was 16.7 kb.

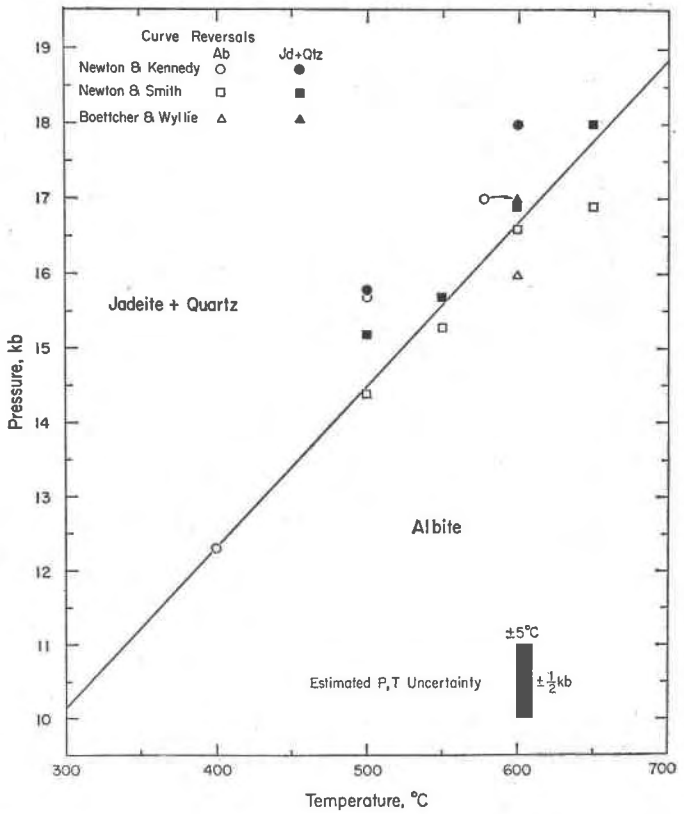

FIG. 3. *P–T* plot of reversals of the reaction albite = jadeite + quartz from Newton and Kennedy (1968), Newton and Smith (1967), and Boettcher and Wyllie (1968). The breakdown curve drawn satisfies the data of Newton and Smith, and Boettcher and Wyllie.

certainties of the experimentally determined curve of albite breakdown.

Curves calculated using equation 5 and pressures obtained from Figure 3 are shown in Figures 2 and 4. Figure 2 shows the ideal system $NaFeSi_3O_8$–$NaAlSi_3O_8$ at 600°, 500°, 400°, and 300°C assuming no solution of iron in albite. Figure 4 shows the iron-rich portion of Figure 2. In addition, Figure 4 shows the 600°C curve with 5 percent substitution of Fe^{+3} for Al in albite assuming ideal mixing on all four tetrahedral sites. Errors in location of the curves may be associated with the uncertainty of the $\Delta\overline{V}$ term and/or the uncertainty in location of the equilibrium pressures of the pure albite–pure jadeite reaction. Errors in those pressures will shift the equilibrium curve in the same direction

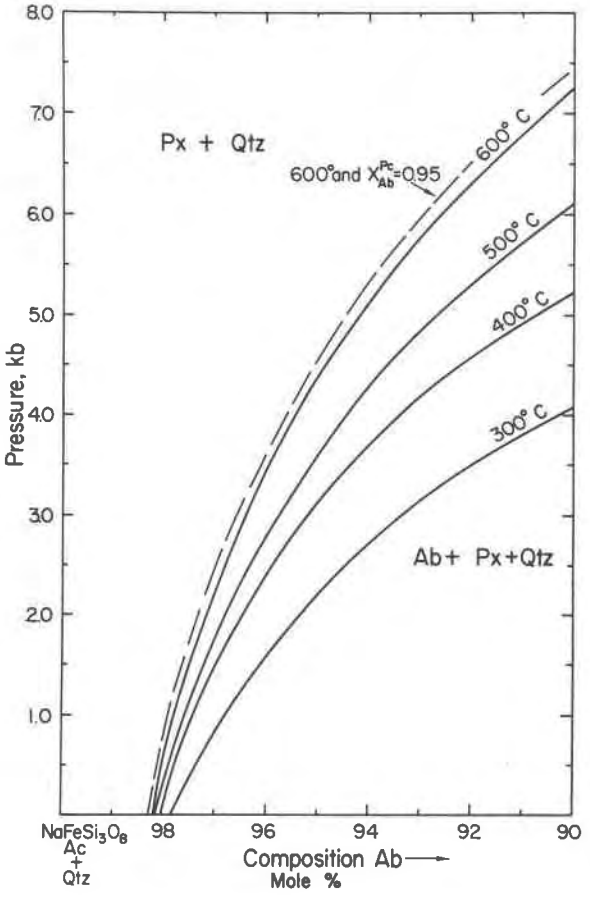

FIG. 4. Ideal relations for the iron-rich portion of the join $NaAlSi_3O_8$–$NaFeSi_3O_8$, for 300°, 400°, 500°, and 600°C assuming albite is chemically pure. Dashed line shows ideal phase relations at 600°C assuming 5 mole percent substitution of Fe^{3+} for Al in albite.

and with the same magnitude as the error itself. The volume uncertainty of ± 0.19 cm^3/mole will shift the curves ± 0.09 mole percent at constant pressure. If high albite rather than low albite had been used in these calculations the $\Delta\overline{V}$ term would be 0.36 cm^3/mole smaller (Robie and others, 1967). This would shift the curve roughly 0.2 mole percent toward albite at constant pressure. If the $\Delta\overline{V}$ for 12 kbar and 400°C were used, the curve would also be shifted 0.5 mole percent toward albite.

Experimental Procedure

Starting Materials

Starting materials usually consisted of oxide mixes, although some runs were seeded with, or consisted entirely of assemblages previously synthesized from these mixes. Reagents used in mixes were: Na_2CO_3: Fisher Lot 790981—dried at 395°C; Fe_2O_3: Fisher Lot 763159—dried at 1000°C; $Al_2O_3 \cdot XH_2O$: Type RH–United Mineral and Chemical Corp.; and, silica class: Corning Glass #7940, crushed, sieved, and acid treated. The water content of the $Al_2O_3 \cdot XH_2O$ reagent was determined to be 31.61 percent. All materials were stored in a vacuum dessicator prior to weighing.

Mixes corresponding to Ac_{100}, Ac_{95}, Ac_{90}, Ac_{80}, and Ac_0 were made. Ac_{95} implies 95 percent $NaFeSi_3O_8$–5 percent $NaAlSi_3O_8$ (mole percent) which is equivalent to a sodic pyroxene of 95 percent $NaFeSi_2O_6$ plus quartz. Runs with compositions other than these were made by combining appropriate amounts of the five mixes. Mixes were ground under acetone in an automated agate mortar and pestle for one hour to achieve homogeneity.

Sample Containers and Apparatus

Iron–bearing charges were run in pure silver capsules, and non–iron–bearing charges were run in pure gold capsules. Runs buffered for oxygen fugacity, f_{O_2}, were contained in gold outer capsules and $Ag_{70}Pd_{30}$ alloy inner capsules and were buffered by the assemblage magnetite–hematite using the methods of Eugster and Wones (1962). Most runs, however, were not buffered. With oxygen–balanced mixes as starting materials, addition of water to the charge should place the runs at an f_{O_2} in the hematite field. In longer runs, sufficient diffusion of hydrogen across the silver capsule wall may have allowed the pressure vessels to exert control on the sample f_{O_2}. The f_{O_2} imposed by Rene 41 vessels is generally considered to be in the Ni–NiO range. Bailey (1969) has shown that acmite is stable in the presence of water for oxygen fugacities above the magnetite–wüstite range. In any case, no differences were noted between buffered and unbuffered runs. Both the charge and the buffer were checked for the presence of water upon opening.

All runs were carried out in cold–seal hydrothermal apparatus first utilized by Tuttle (1949) and essentially identical to the system described by Ernst (1968, p. 33–35). Pressures were measured to the nearest bar on a Heise bourdon tube 7.7 kbar gauge with 10 bar divisions. The gauge was calibrated at the factory against a dead–weight piston gauge, and set to read 0.0 bars at atmospheric pressure. The maximum pressure variation noted during runs was ±.15 kbar, but most were within ±.05 kb. Temperature measurements were made by use of bare–wire chromel–alumel thermocouples held in a ceramic sheath inserted into the thermocouple well of the pressure vessels. Temperatures in open vessels for five furnaces were calibrated against the 1 atmosphere melting point of NaCl (800.5°C). Temperature variations of ±5°C were noted during the runs.

Phase Identification and Characterization

Procedures

Run products listed in Table 1 were examined with the petrographic microscope and X–ray powder diffraction. The electron microprobe was not used simply because the grain sizes were generally too small. Optical properties were

TABLE 1: Run Summary

Run #	Comp.[a]	Starting Materials[b]	T(°C)	P(kb)	Dur. (Days)	Products Identified[c]
41	98	M	400	4.0	44	P+Q
42	95	M	400	4.0	44	P+Q
43	90	M	400	4.0	44	P+Q+Ab
51	100	M	400	4.0	20	P+Q
52	95	M	400	2.0	20	P+Q
53	95	M	400	4.5	20	P+Q
20	100	M	500	4.0	53	P+Q
22	100	M	500	4.0	12	P+Q
25	98	MS	500	4.0	11	P+Q
26	96	MS	500	4.0	11	P+Q
27	94	MS	500	4.0	11	P+Q+Ab
28	92	MS	500	4.0	11	P+Q+Ab+A
37	95	M	500	1.0	17	P+Q+Ab
38	95	M	500	2.0	17	P+Q+Ab
40	95	M	500	4.5	17	P+Q
48	100	M	500	4.0	13	P+Q
49	95	M	500	4.0	13	P+Q
50	90	M	500	4.0	13	P+Q+Ab
19	95	M	600	4.0	53	P+Q
30	80	M	600	4.0	11	P+Q+Ab
34	80	M	600	1.0	11	P+Q+Ab
45	90	M	600	4.0	40	P+Q+Ab
46	92	M	600	4.0	40	P+Q+Ab
47	98	M	600	4.0	40	P+Q
60	92	S	600	4.0	25	P+Q+Ab
61	95	S	600	4.0	25	P+Q+Ab
62	97	S	600	4.0	25	P+Q
63	99	S	600	4.0	25	P+Q

[a] Mole % $NaFeSi_2O_6$ in bulk composition of run

[b] M = oxide mix; MS = oxide mix (Ac_{100}) plus synthetic albite ($Ac_{0.0}$); S = synthetic acmite + quartz (Ac_{100}) plus synthetic albite($Ac_{0.0}$)

[c] P = pyroxene; Q = quartz; Ab = albite; A = amphibole

compared to those listed in Winchell and Winchell (1964). As optical detection of albite in runs containing small quantities of that phase was virtually impossible, X-ray powder diffraction scans were utilized for identification. All scans were carried out on a Norelco powder diffractometer equipped with a graphite crystal monochrometer, using Cu radiation. For purposes of identification, scans of 1° and 2° 2θ/min. were sufficient. Two-theta values for reflections used in refining the cell parameters of the run phases were obtained by making two oscillations (4 scans) between 12° and 60° 2θ at 1/2° 2θ/min., with synthetic $MgAl_2O_4$ spinel ($a = 8.083$ Å) supplied by G. V. Gibbs, as an internal standard. Reflections were indexed by comparison of the patterns with those in Borg and Smith (1969). Calculation of the cell parameters and least-squares refinement was accomplished with the aid of the program written by Evans, Appleman, and Handwerker (1963). Cell parameters are reported showing one standard error as calculated by the program.

In the 500–600°C range, runs of 7–10 days showed almost complete reaction from oxide mix to pyroxene, quartz ± albite. Large grains contained some inclusions, but the smaller grains appeared homogeneous. Products appeared to be in equilibrium on the basis of lack of zoning and no identifiable reaction rims. Synthesis runs contained excess gas which was largely CO_2 given off in the reaction of Na_2CO_3. A glass with an index of refraction close to 1.52 was identified in a number of runs. This glass comprised less than 1 percent of the runs and is presumed to be a quench product from solids dissolved in the aqueous vapor during the runs.

Acmitic Pyroxene

Acmitic pyroxene was easily identified optically and with X-ray methods. Optically, it appeared as needles ranging in length from 5μ to 100μ, the large majority of the grains being in the 5μ–20μ range. The smaller grains were homogenous and slightly pleochroic between light green and yellow-green. Pyroxene needles often coated larger quartz grains and in some cases appeared to be partially embedded in the larger grains. Approximate refractive indices obtained were consistent with those given by Winchell and Winchell (1964) as were extinction angles. X-ray patterns were consistent with those given by Borg and Smith (1969) with all peaks of relative intensity of 3 or greater being identified up to 53° 2θ. Cell parameters were calculated from measurement of 10 reflections (Table 2).

Albite

Albite was identified optically only in 600° runs of composition Ac_{90} and below. In these runs albite occurred as "plate-like" crystals often massed in large aggregates easily distinguishable from euhedral and subhedral quartz grains, and pyroxene in an oil of $n = 1.78$. In runs other than those noted above, albite occurred as anhedral grains in the 5μ–10μ range and could not be clearly distinguished from quartz. X-ray methods were relied on almost entirely for identification of albite.

Adequate data for cell refinement could be obtained for only three albites due to the extensive overlap of pyroxene, quartz, and albite peaks. Table 3 gives cell parameters and $\Psi(\Delta 2\theta \mathrm{CuK}_\alpha = 2\theta_{131} - 2\theta_{1\bar{3}1})$ for albites from this study along with data from Martin (1969), Smith (1956), and Starkey and Wainwright (1969) (from Martin, 1970). For comparison, unit cell volumes and Ψ for high and low albite were calculated from the data of Smith and Starkey and Wainwright, respectively. Both relative positions on the *bc* plot (Δbc) and Ψ indicate a high–intermediate structural

TABLE 2: Pyroxene Cell Parameters

Run #	a(Å)	b(Å)	c(Å)	β	V(Å^3)
41	9.649(3)	8.790(3)	5.292(2)	107°24.1'(1.7)	428.2(2)
42	9.648(3)	8.790(2)	5.294(2)	107°23.5'(1.8)	428.4(2)
43	9.646(9)	8.769(19)	5.295(4)	107°21.5'(3.8)	427.5(5)
51	9.659(3)	8.800(3)	5.298(2)	107°24.9'(1.9)	429.7(2)
52	9.643(3)	8.783(3)	5.292(2)	107°23.4'(1.9)	427.7(2)
53	9.642(4)	8.787(4)	5.294(2)	107°24.0'(2.5)	428.0(2)
20	9.654(2)	8.797(2)	5.297(3)	107°25.6'(1.8)	428.7(1)
22	9.655(3)	8.797(4)	5.293(3)	107°21.1'(1.7)	429.1(2)
25	9.651(5)	8.786(5)	5.304(6)	107°27.4'(3.8)	429.1(3)
26	9.654(2)	8.785(3)	5.302(3)	107°29.0'(1.9)	428.9(2)
27	9.651(3)	8.781(3)	5.299(4)	107°28.6'(2.7)	428.3(2)
28	9.654(2)	8.783(2)	5.301(3)	107°29.8'(1.9)	428.8(2)
37	9.648(2)	8.789(2)	5.294(1)	107°23.4'(1.2)	428.4(1)
38	9.646(3)	8.786(3)	5.292(2)	107°23.1'(2.0)	428.0(2)
40	9.644(3)	8.785(3)	5.293(2)	107°25.2'(1.9)	427.9(2)
48	9.655(3)	8.799(3)	5.296(2)	107°24.8'(1.9)	429.3(2)
49	9.645(3)	8.785(2)	5.294(2)	107°25.2'(1.8)	427.9(2)
50	9.644(4)	8.778(3)	5.291(2)	107°25.1'(2.3)	427.4(2)
19	9.645(4)	8.784(3)	5.293(2)	107°25.2'(2.5)	427.9(2)
30	9.648(4)	8.788(3)	5.293(3)	107°23.6'(4.1)	428.3(3)
34	9.650(3)	8.786(2)	5.294(1)	107°24.6'(1.6)	428.3(1)
45	9.643(3)	8.784(2)	5.294(1)	107°25.1'(1.5)	427.8(1)
46	9.646(5)	8.789(4)	5.295(3)	107°24.4'(2.7)	428.4(2)
47	9.653(5)	8.793(4)	5.296(3)	107°26.3'(2.7)	428.9(2)

TABLE 3: Albite Cell Parameters

Comp.	T(°C)	P(kb)	a(Å)	b(Å)	c(Å)	α	β	γ	V(Å³)	Y
100[a]	600°	4.0	8.157(11)	12.858(11)	7.123(5)	93°31.9'(8.0)	116°32.1'(8.7)	89°48.5'(9.2)	666.89(81)	1.785
80[a]	600°	4.0	8.152(7)	12.868(14)	7.125(3)	93°37.3'(6.0)	116°30.6'(5.6)	89°44.6'(5.0)	667.29(76)	1.798
100[a]	600°	1.0	8.155(13)	12.856(12)	7.119(6)	93°36.8'(8.9)	116°31.5'(9.6)	89°50.6'(7.6)	666.22(90)	1.845
Ab_{100}[b]	600°	1.0								1.816
Ab_{100}[b]	600°	3.5								1.792
Low Ab[c]			8.133	12.781	7.155	94°17'	116°37'	87°44'	663.0[e]	1.136[f]
High Ab[d]			8.171	12.872	7.108	93°28'	116°23'	90°20'	668.1[f]	2.110[e]

[a]% $NaAlSi_3O_8$ in bulk comp. of run, this study

[b]Martin (1969)

[c]Starkey and Wainwright (1969)

[d]Smith (1956)

[e]Calculated using cell parameters of Starkey and Wainwright (1969)

[f]Calculated using cell parameters of Smith (1956)

state for all three albites with the Al distribution being approximately: $Al_{T_1 0} = .36$, $Al_{T_1 m} = Al_{T_2 0} = Al_{T_2 m} = 0.21$ (Stewart and Ribbe, 1969).

The question now arises whether the albite crystallized in the iron-bearing charge contains iron. The *b* cell edge is the most sensitive cell parameter to iron substitution (Ribbe, personal comm.). Although the standard errors are rather large, the *b* cell edge of the albite synthesized in the iron-bearing system is on the order of 0.01 Å larger than those in the iron-free system. Also, within one standard deviation, the albites from the iron-free runs lie on the high-low albite "join" on the *bc* plot, whereas that of the iron-bearing run lies off this "join," and suggests the presence of iron in the structure.

Finally, comparison of the cell volumes of sanidine and iron-sanidine, or microcline and iron-microcline (Robie and others, 1967), shows differences of the order of 25 to 26 Å³. If similar differences were to apply to albite and an iron-albite, then the data in Table 3 indicate that the amount of iron, if present at all, must be less than 4–5 mol percent. Newton and Smith (1967) reported averaged values of 1–2 wt. percent iron (3–6 mole percent iron albite) in electron microprobe analyses of albites synthesized at 15–17 kbar in this system, but did not claim that these represented equilibrium.

Quartz

Optically, quartz appeared in several different forms. In 600° runs in which albite was not detected, quartz occurred both as large (100–200μ) prismatic grains with pyramidal terminations and also as anhedral grains up to 50μ. In 500°C and 400°C runs and runs in which albite was detected, quartz occurred as very small anhedral grains (5μ–10μ) and was virtually impossible to distinguish optically from albite. Quartz was easily identified in the X-ray powder patterns.

Figure 5 is a plot of cell volume vs. temperature for quartz present in the runs of this study. Cell refinements were based upon only three peaks. The plot shows that cell volumes of all quartz present is roughly in accord with the volume of low quartz: 113.01 ± .01 Å (Robie and others, 1967). The tendency towards somewhat larger cell volumes might indicate solution of impurities in the quartz. Runs were in the stability field of low quartz except for the run at

600°C and 1.0 kbar which lies near or in the high quartz field (Tuttle and Bowen, 1958, p. 29). If the larger cell volumes in Figure 5 are indeed due to the presence of impurities, it would have been reasonable to expect greater solution in a run penetrating the high quartz field (cell volume 118.15 ± .06 Å, Robie and others, 1967), which might be reflected in an even larger cell volume upon inversion to low quartz. However, the cell volume of the 600°C, 1.0 kbar run shows no special features.

Amphibole

A gruneritic amphibole was detected in a run of composition Ac_{02} at 500°C and 4.0 kb. Starting materials were an oxide mix seeded with synthetic albite.

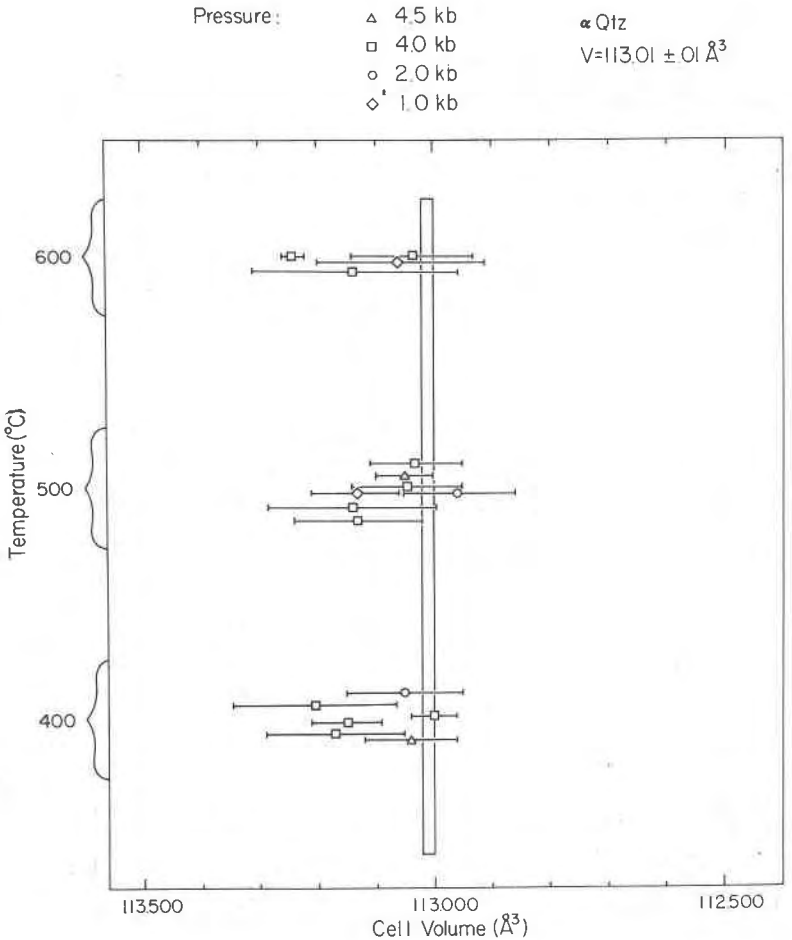

FIG. 5. Plot of cell volume of quartz present in runs vs. temperature. Cell volume of low (α) quartz from Robie and others (1967) is also shown.

TABLE 4: Amphibole comparisons

	Synthetic Amphibole This Study		Synthetic Amphibole[a] Kopp and Harris (1967)		Grunerite #1[b] Klein (1964)		Riebeckite Borg and Smith (1969)	
hKl	d(Å)	I/Io	d(Å)	I/Io	d(Å)	I/Io	d(Å)	I/Io
110	8.385	100	8.33	100	8.330	100	8.429	100
131	3.470	40	3.47	40	3.466	55	3.419	12
240	3.282	45	3.29	40	3.278	50	3.276	3
310	3.081	90	3.08	75	3.071	80	3.130	22
151	2.772	100	2.78	75	2.7655	90	2.724	29
061	2.643	80	2.65	50	2.639	70	2.600	9

Cell Parameters

a = 9.549(13)Å

b = 18.513(29)Å

c = 5.245(31)Å

β = 100°38.29'(23.42)

V = 911.26(42)Å^3

[a] Gruneritic amphibole synthesized in system SiO_2-NaOH-Fe-H_2O.

[b] Composition $(Fe_{6.17}, Mg_{0.77}, Mn_{0.05}, Ca_{0.06})\ Si_8O_{22}(OH,F)_2$

Optically it occurred as individual grains approximately 30μ long and 1μ–3μ wide. Grains were not generally associated with the pyroxene, and were nearly invisible in an oil of $n = 1.70$. Table 4 summarizes the data obtained for this amphibole and gives some comparisons. It appears to be gruneritic with solution of some riebeckite or ferroglaucophane component. Its stability relations were not investigated.

Experimental Results

Determination of Phase Boundary

Figure 6 shows X–ray powder patterns of mixtures of 1, 3, 5, and 8 mole percent synthetic albite ($Ac_{0.0}$) in synthetic acmite and quartz (Ac_{100}). Also shown are the equivalent bulk compositions assuming the equilibrium boundary lies at Ac_{95}, *i.e.*, the bulk composition Ac_{94} will contain approximately 1 percent albite if the boundary lies at Ac_{95}. From Figure 6, it would seem that 1 percent of well–crystallized albite should be detectable in powder patterns of the runs. These calibration mixtures were used in the interpretation of powder patterns of other runs. It should be noted that the grain size of the materials (and presumably the structural state of the albite) used in the calibration mixtures is equivalent to that of the run products.

600°C Runs. X–ray powder patterns of products of runs made from oxide mixes at 600°C and 4.0 kbar are shown in Figure 7. Albite is

definitely present in the Ac_{92} run and is either absent or present in amounts less than 1 percent in the Ac_{95} run. Figure 8 is a plot of cell parameters (a, b, and V) for the pyroxenes shown in Figure 7, from synthesis runs of Ac_{80} at 600°C and 4.0 kbar, and of Ac_{100}. The values for Ac_{100} are averages of cell dimensions of four pyroxenes synthesized at 4.0 kbar in the 400–600°C range, and are in agreement with those of Nolan and Edgar (1963) and Gilbert (1967). The portion of the curve from Ac_{100} to approximately Ac_{95} indicates a change in pyroxene composition, and its slope is in agreement with that obtained by Gilbert (1967). The horizontal portion of the curve suggests that the equilibrium boundary has been crossed and that an increase in $NaAlSi_3O_8$ component increases the amount of albite present but does

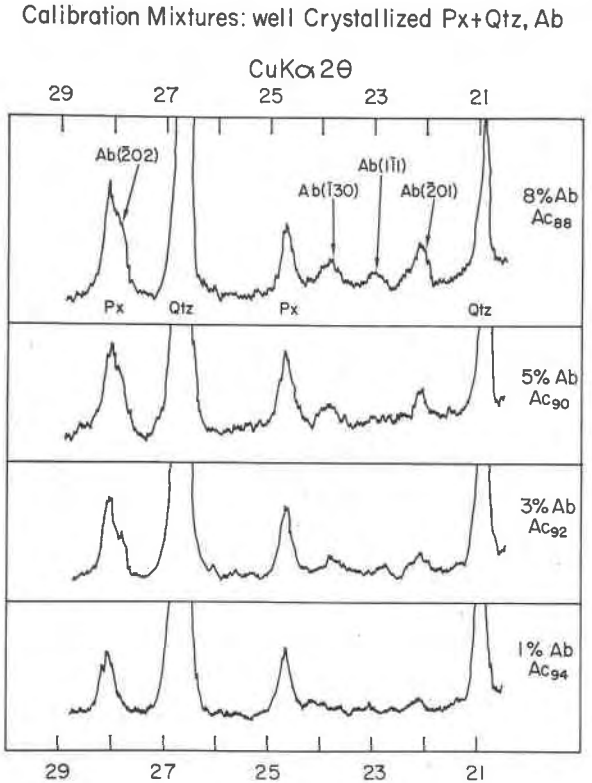

FIG. 6. X-ray powder patterns of mixtures of well-crystallized pyroxene plus quartz, with varying amounts of well-crystallized albite. Composition symbols represent the bulk composition of the run which will contain the indicated amount of albite if the equilibrium boundary lies at Ac_{95}.

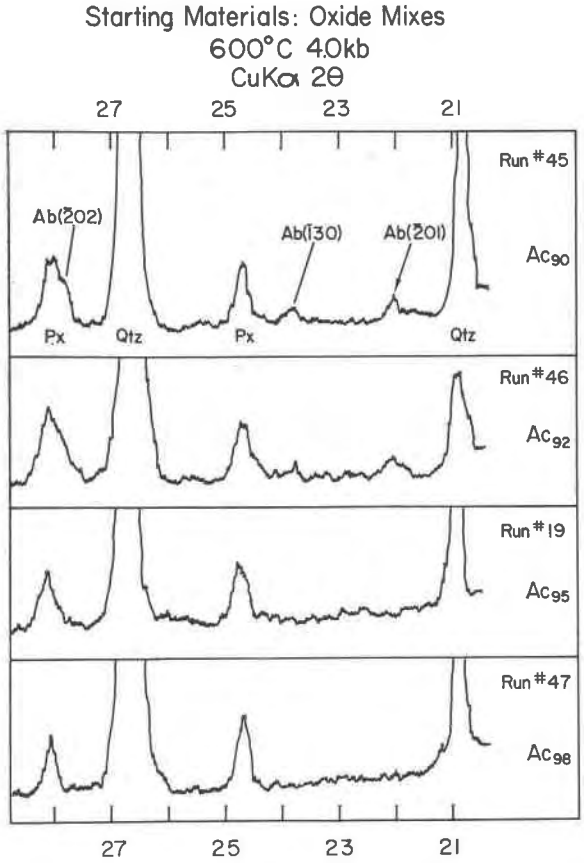

FIG. 7. X–ray powder patterns of products of runs at 600°C and 4.0 kbar. Starting materials were oxide mixes.

not change the pyroxene composition. On the basis of these data, the phase boundary is assumed to lie between Ac_{96} and Ac_{95} at 600°C and 4.0 kbar, which is in accord with Figure 4. In addition, Figure 9 shows X–ray powder patterns for products of a series of runs of synthetic pure albite and synthetic pure acmite plus quartz at 600°C and 4.0 kbar. The presence of albite in Ac_{95} (Figure 9, #61) may be explained as a consequence of the fact that the bulk composition lies very close to the phase boundary. In such a case, the driving force for the reaction of albite with the pyroxene would be small and some excess, unreacted albite might be expected. These results are all consistent with location of the phase boundary at a composition more iron–rich than Ac_{95}.

500°C Runs. X–ray powder patterns for products of runs at 500°C and 4.0 kbar for compositions prepared by mixing the appropriate amount of synthetic albite with Ac_{100} mix are shown in Figure 10. Albite has definitely disappeared in the Ac_{98} and Ac_{96} runs, but is still present in the Ac_{94} run. This indicates the phase boundary curve lies between Ac_{96} and Ac_{94} at 500°C and 4.0 kbar. X–ray patterns of synthesis runs of Ac_{95} at 500°C and pressures of 1.0, 2.0, 4.0, and 4.5 kbar showed albite present in the 1.0 and 2.0 kbar runs and absent in the higher pressure runs. The cell parameters of the pyroxenes in these runs indicate a change in composition between 1.0 and 2.0 kbar but no change for higher pressures and apparently reflect the slope of the phase boundary. Although this change is very slight, it is consistent with location of the boundary between Ac_{95} and Ac_{94}. Thus, the boundary should lie between Ac_{95} and Ac_{94} on the basis of all runs at 500°C, which is also in accord with Figure 4.

400°C Runs. Runs at 400°C and pressures from 1.0 to 4.5 kbar were generally poorly crystallized in runs up to six weeks. The data were

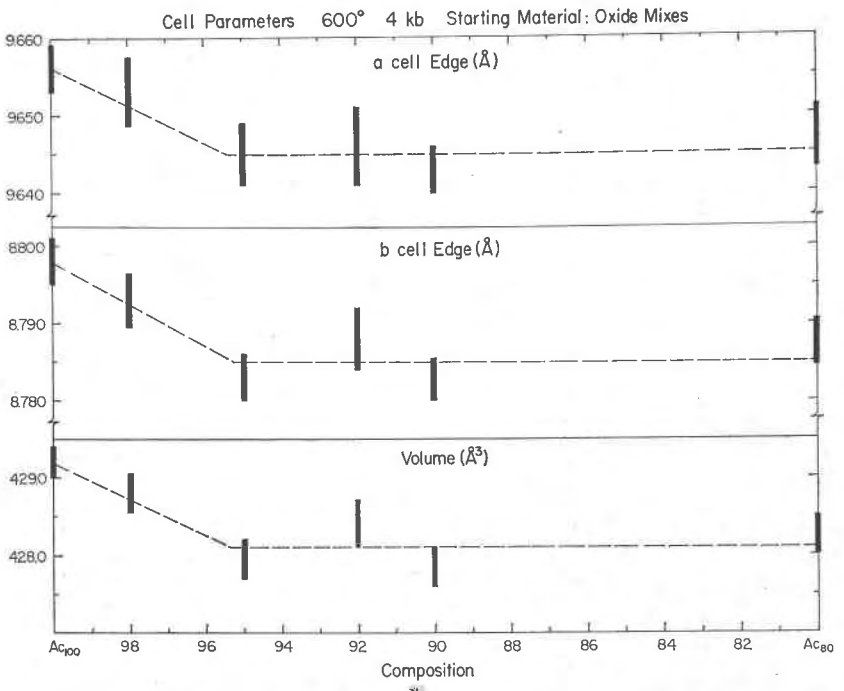

FIG. 8. Plot of cell parameters of pyroxenes vs. bulk composition of runs made at 600°C and 4.0 kbar from oxide mixes. The parameters of Ac_{100} are averages of four pyroxenes synthesized at 4.0 kbar in the range 400–600°C.

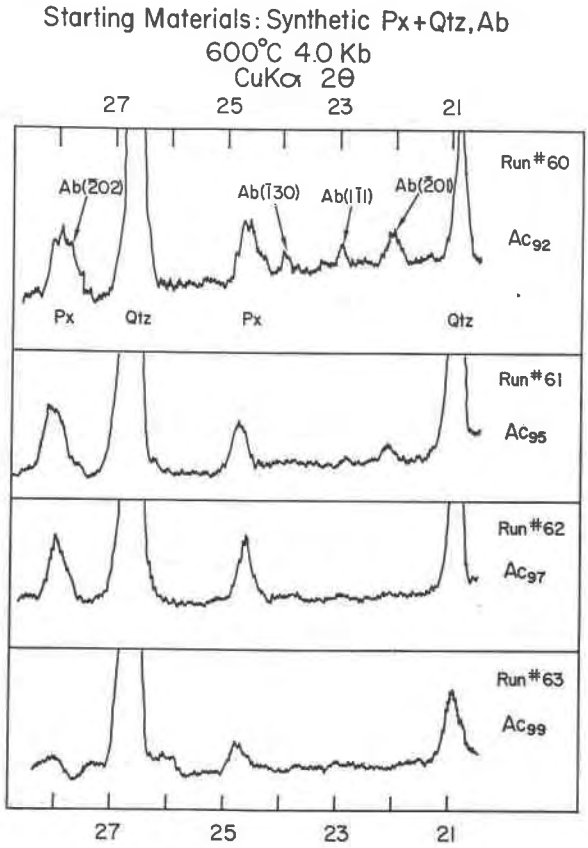

FIG. 9. X—ray powder patterns of products of runs made at 600°C and 4.0 kbar. Starting materials were synthetic pyroxene plus quartz, and synthetic albite.

only sufficient to bracket the phase boundary between Ac_{95} and Ac_{90} at 400°C.

Discussion of the Phase Boundary

A comparison of the experimental approach with the ideal phase diagram shows consistency between the two approaches. Assuming that the system is ideal, the calculated curves drawn in Figures 2 and 4 represent a good approximation to the boundaries of 500°C and 600°C at 4.0 kbar based on run data. An error of ±1 mole percent in location of the boundary in this manner shifts the pressure of pure albite breakdown ±0.75 kbar. This is approximately equal to the pressure uncertainties in piston–cylinder apparatus. As the calcu-

lated curves depend upon knowledge of the pressure at which pure albite breaks down, the breakdown curve as drawn in Figure 4 represents a close approximation to the true equilibrium breakdown curve assuming ideality. Since all previous studies of albite breakdown in the 500–600°C temperature range have been carried out in solid pressure medium devices, the results of the hydrothermal study may be of value in confirmation of these studies.

Finally, it should be noted that the phase boundary has not been reversed, that is, one phase Fe–Al pyroxenes were not synthesized at high pressure in the field pyroxene plus quartz and then run at lower pressure where albite exsolves. However, the runs made from the same side of the reaction using both mixes directly and using previously synthesized albite, acmite, and quartz gave consistent and concordant results.

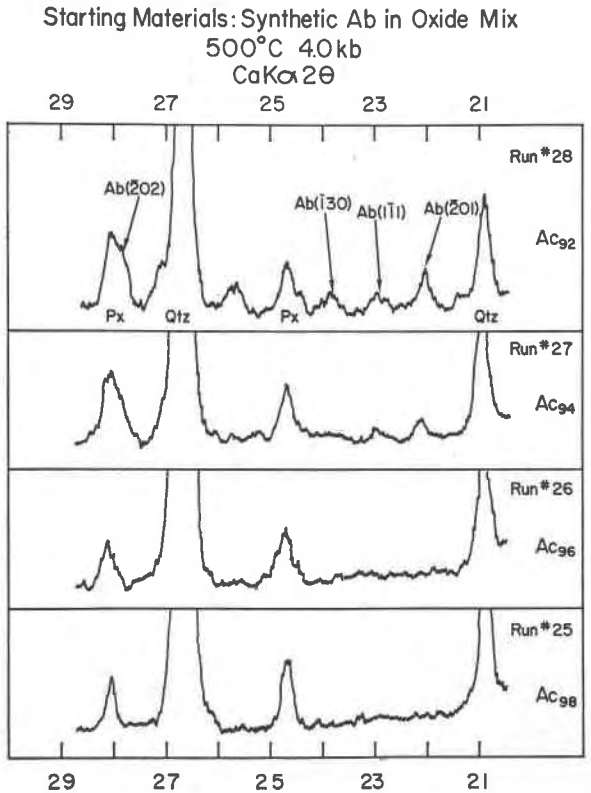

FIG. 10. X-ray powder patterns of products from runs at 500°C and 4.0 kbar. Starting materials were oxide (Ac_{100}) seeded with synthetic albite.

Geological Applications

Iron-rich sodic pyroxenes occur in a wide range of geological environments. Acmite, or aegirine as the green to black form of $NaFeSi_2O_6$ is called, has been reported in plutonic, hypabyssal, and volcanic igneous rocks, pegmatites, metamorphic rocks, and in hydrothermal, metasomatic, and diagenetic environments.

In silica-saturated environments, the maximum solubility of jadeite component in sodic pyroxenes will be determined by the curves in Figure 2. In a silica-undersaturated environment, the solubility of jadeite is limited by reaction (2), from which a set of curves similar to Figure 1 may be calculated using an ideal solution model. The $\Delta\overline{V}$ term of reaction (2) is essentially the same as for reaction (1), but the P–T curve of jadeite breakdown in the silica-undersaturated system is roughly 5 kbar lower than in the silica-saturated system (see Hlabse and Kleppa, 1968, for a summary of each system). Thus jadeite should be appreciably more soluble in acmite in the silica-undersaturated environment.

Acmitic pyroxenes are a late crystallizing phase in plutonic alkali magmas and are common constituents in quartz syenites, syenites, nepheline syenites, and syenite pegmatites (Deer and others, 1963). Available analyses of pyroxenes from such environments (Deer and others, 1963, Vol. 2, table 12; Grout, 1946; Sutherland, 1969) show significantly larger proportions of jadeite component in acmitic pyroxenes from silica-undersaturated environments.

Composition of sodic pyroxenes coexisting with quartz and albite might be used to indicate pressures of formation if temperatures can be estimated. Grout (1946) reports acmite occurring as disseminated grains in taconites and in veins coexisting with quartz and "silicic plagioclase" in rocks of the Cuyuna Range, Minnesota. An analysis of a vein type acmite shows the $M(1)$ site to contain .954 Fe^{3+}, .036 Al, and .035 others, plus 0.12 Al^{IV}. If we use the convention, $Fe^{3+}/[Fe^{3+} + (Al^{VI} - Al^{IV})]$ = percent acmite in the acmite–jadeite part of the solution, then the vein pyroxene is 97.5 percent acmite. On the basis of Grout's claim that the deposits are hypothermal (300–500°C) and Figure 4 of this study, the pressure of final equilibration of the assemblage would lie in the range 1/4 to 1 kbar.

In blueschist metamorphic rocks of the Franciscan Group in California, iron-rich sodic pyroxenes occur primarily in metacherts (Coleman and Clark, 1968). The only available analyses of such pyroxenes are those of Onuki and Ernst (1969), who give analyses of two acmitic pyroxenes from metachert and siliceous ferruginous shale from a Laytonville, California quarry. Cation proportions of $M(1)$ sites in the

metachert pyroxene are: .883 Fe^{3+}, .022 Al, and .120 others, plus .004 Al^{IV} which gives 97.8 percent acmite. $M(1)$ cation proportions in the pyroxene from the metashale are: .677 Fe^{3+}, .079 Al, and .235 others, plus .017 Al^{IV} which gives 91.8 percent acmite. Both pyroxenes coexist with quartz but not albite. Chesterman (1966) notes that the rocks of the Laytonville quarry are similar to the type III metamorphic rocks of Coleman and Lee (1963). Coleman (1967) and Taylor and Coleman (1968) suggest temperatures of 200–300°C would be appropriate for formation of type III rocks. On the basis of these data and Figure 4 of this study, pressure of formation of the Laytonville rocks must have been greater than approximately 3.5 kbar. This pressure represents the lower limit of formation because albite is not present and therefore is consistent with the somewhat higher pressure estimates of Coleman (1967) and Ernst and others (1970).

The situations discussed above illustrate simplified interpretations as no account is taken of the effects of other components on the pyroxene phase relations. Nevertheless, the discussion indicates how estimation of pressures of formation by means of sodic pyroxene composition could become a valuable tool as more analyses become available. This is especially true in the case of alkali igneous rocks, in which sodic pyroxenes commonly occur. It is essential, however, that the presence or absence of coexisting albite and/or quartz definitely be noted.

Acknowledgements

Gratitude is expressed to W. G. Ernst, E. S. Essene, J. F. Hays, and R. C. Newton for critically reviewing the manuscript, and also to P. H. Ribbe for reviewing the discussion involving albite. F. D. Bloss, G. V. Gibbs, and D. A. Hewitt reviewed an earlier version of the manuscript. This study was supported by NSF grant #GA-12479/Gilbert.

References

Bailey, D. K. (1969) The stability of acmite in the presence of H_2O. *Amer. J. Sci.* **267A**, 1–16.

Birch, F., and P. LeComte (1960) Temperature-pressure plane for albite composition. *Amer. J. Sci.* **258**, 209–217.

Boettcher, A. L., and P. J. Wyllie (1968) Jadeite stability measured in the presence of silicate liquids in the system $NaAlSiO_4$–SiO_2–H_2O. *Geochim. Cosmochim. Acta*, **32**, 999–1012.

Borg, I. Y., and D. K. Smith (1969) Calulated X-ray powder patterns for silicate minerals. *Geol. Soc. Amer. Mem.* **122**, 896 pp.

Chesterman, C. W. (1966) Mineralogy of the Laytonville Quarry, Mendocina Country, California. *Calif. Div. Mines Geol. Bull.* **190**, 503–508.

Clark, J. R., D. E. Appleman, and J. J. Papike (1969) Crystal-chemical characterization of clinopyroxenes based on eight new structure refinements. p. 31–50, *Mineral. Soc. Amer. Spec. Pap. No.* **2**, 314 pp.

———, AND J. J. PAPIKE (1968) Crystal-chemical characterization of omphacites. *Amer. Mineral.* 53, 840–868.

CLARK, S. P. (ed.) (1966) Handbook of physical constants. *Geol. Soc. Amer. Mem.* 97, 587 pp.

COLEMAN, R. G. (1967) Glaucophane schists from California and New Caledonia. *Tectonophysics,* 4, 479–498.

———, AND J. R. CLARK (1968) Pyroxenes in the blueschist facies of California. *Amer. J. Sci.* 266, 43–59.

———, AND D. E. LEE (1963) Glaucophane-bearing metamorphic rock types of the Cazadero area, California. *J. Petrology,* 4, 260–301.

DEER, W. A., R. A. HOWIE, AND M. A. ZUSSMAN (1963) *Rock Forming Minerals, Vol.* 2, *Chain Silicates.* Longmans, Green, and Co. Ltd., London. 379 pp.

DOBRETSOV, N. L. (1962) Miscibility limits and mean compositions of jadeite pyroxenes. *Akad. Nauk. S.S.S.R. Dokl.* 146, 676.

ERNST, W. G. (1968) *Amphiboles: Crystal Chemistry, Phase Relations, and Occurrence.* Springer-Verlag, New York, 125 pp.

———, Y. SEKI, H. ONUKI, AND M. C. GILBERT (1970) Comparative study of low-grade metamorphism in the California Coast ranges and the outer metamorphic belt of Japan. *Geol. Soc Amer. Mem.* 124, 276 pp.

ESSENE, E. S., AND W. S. FYFE (1967) Omphacite in California metamorphic rocks. *Contrib. Mineral. Petrology,* 15, 1–23.

EUGSTER, H. P., AND D. R. WONES (1962) Stability relations of the ferruginous biotite, annite. *J. Petrology,* 3, 82–125.

EVANS, H. T., D. E. APPLEMAN, AND D. S. HANDWERKER (1963) The least squares refinement of crystal unit cells with power diffraction data by an automated computer indexing method. *Amer. Crystallogr. Assoc. Meet., Cambridge, Mass., (Prog. Abstr.)* 42.

GILBERT, M. C. (1967) X-ray properties of jadeite–acmite pyroxenes. *Carnegie Inst. Wash. Year Book,* 66, 374–375.

——— (1969) High pressure stability of acmite. *Amer. J. Sci.* 267A, 145–159.

GROUT, F. F. (1946) Acmite occurrences in the Cuyuna Range, Minnesota. *Amer. Mineral.* 31, 125–131.

HLABSE, T., AND O. J. KLEPPA (1968) The thermochemistry of jadeite. *Amer. Mineral.* 53, 1281–1292.

JOHANNES, W., P. M. BELL, H. K. MAO, A. L. BOETTCHER, D. W. CHIPMAN, J. F. HAYS, R. C. NEWTON, AND F. SEIFERT (1971) An interlaboratory comparison of piston–cylinder pressure calibration using the albite-breakdown reaction. *contrib. Mineral. Petrology,* 32, 24–38.

KLEIN, C. (1964) Cummingtonite–grunerite series: A chemical, optical, and X-ray study. *Amer. Mineral.* 49, 963–982.

KOPP, O. C., AND L. A. HARRIS (1967) Synthesis of grunerite and other phases in the system SiO_2–NaOH–Fe–H_2O. *Amer. Mineral.* 52, 1681–1688.

MARTIN, R. F. (1969) The hydrothermal synthesis of low albite. *Contrib. Mineral. Petrology,* 23, 323–339.

——— (1970) Cell parameters and infrared absorption of synthetic high to low albites. *Contrib. Mineral. Petrology,* 26, 62–74.

NEWTON, M. S., AND G. C. KENNEDY (1968) Jadeite, analcite, nepheline, and albite at high temperatures and pressures. *Amer. J. Sci.* 266, 728–735.

NEWTON, R. C., AND J. V. SMITH (1967) Investigations concerning the breakdown of albite at depth in the earth. *J. Geol.* 75, 268–286.

NOLAN, J., AND A. D. EDGAR (1963) An X-ray investigation of synthetic pyroxenes in the system acmite-diopside-water at 1000 kg/cm^2 water vapour pressure. *Mineral Mag.* **33**, 625–634.

ONUKI, H., AND W. G. ERNST (1969) Coexisting sodic amphiboles and sodic pyroxenes from blueschist facies metamorphic rocks. *Mineral. Soc. Amer., Spec. Pap.* **2**, 241–249.

PREWITT, C. T., AND C. W. BURNHAM (1966) The crystal structure of jadeite, $NaAlSi_2O_6$. *Amer. Mineral.* **51**, 956–975.

RICHARDSON, S.W., P. M. BELL, AND M. C. GILBERT (1968) Kyanite–sillimanite equilibrium between 700° and 1500°C. *Amer. J. Sci.* **266**, 513–544.

ROBIE, R. A., P. M. BETHKE, AND K. M. BEARDSLEY (1967) Selected X-ray crystallographic data; Molar volumes and densities of minerals and related substances. *U.S. Geol. Surv. Bull.* **1248**, 87.

SHANNON, R. D., AND C. T. PREWITT (1969) Effective ionic radii in oxides and fluorides. *Acta Crystallogr.*, **B-25**, 925–946.

SMITH, J. V. (1956) The powder patterns and lattice parameters of plagioclase feldspars. I. The soda-rich plagioclases. *Mineral. Mag.* **31**, 47–58.

STARKEY, J., AND J. E. N. WAINWRIGHT (1969) Uber die stucktur des tiefalbite aus gluften in den glaukophanschiefern Kaliforniens. *Deutsch. Mineral. Ges., Prog., Ann. Meet.*, **51**.

STEWART, D. B., AND P. H. RIBBE (1969) Structural explanation for variation in cell parameters of alkali feldspar with Al/Si ordering. *Amer. J. Sci.* **267A**, 444–462.

SUTHERLAND, D. S. (1969) Sodic amphiboles and pyroxenes from fenites in eastern Africa. *Contrib. Mineral. Petrology*, **24**, 114–130.

TAYLOR, H. P., AND R. G. COLEMAN (1968) O^{18}/O^{16} ratios of coexisting minerals in glaucophane-bearing metamorphic rocks: *Geol. Soc. Amer. Bull.* **79**, 1727–1756.

TUTTLE, O. F. (1949) Two pressure vessels for silicate–water studies. *Geol. Soc. Amer. Bull.* **60**, 1727–1729.

———, AND N. L. BOWEN, (1958) Origin of granite in the light of experimental studies in the system $NaAlSi_3O_8$–$KAlSi_3O_8$–SiO_2–H_2O. *Geol. Soc. Amer. Mem.* **74**, 153 pp.

WARREN, B. E., AND W. L. BRAGG (1928) The structure of diopside $CaMg(SiO_3)_2$. *Z. Kristallogr.* **69**, 168.

WINCHELL, A. N., AND H. WINCHELL (1964) *The Microscopial Characters of Artificial Inorganic Substances: Optical Properties of Artificial Minerals.* Academic Press, New York. 439 pp.

Manuscript received, November 15, 1971; accepted for publication, March 27, 1972.